

# A GENERIC PUSHBROOM SENSOR MODEL FOR HIGH-RESOLUTION SATELLITE IMAGERY APPLIED TO SPOT 5, QUICKBIRD AND ALOS DATA SETS

T. Weser\*, F. Rottensteiner, J. Willneff, C. Fraser

Cooperative Research Centre for Spatial Information, Department of Geomatics,  
The University of Melbourne VIC 3010, Australia - (tweser, franzr, jochenw, c.fraser)@unimelb.edu.au

Commission I, WG I/5

**KEY WORDS:** Pushbroom sensor, SPOT 5, QuickBird, ALOS PRISM

## ABSTRACT:

A new generic pushbroom sensor model for high-resolution satellite images is presented. The sensor orbit and attitudes are modelled by splines. In order to determine the parameters of the orbit and attitude splines, direct observations for the satellite orbits and attitudes that are provided by the data vendors in metadata files are considered. As these direct observations are usually contaminated by systematic errors, the pushbroom sensor model also requires a correction model for these systematic errors. Unfortunately, the definitions of file formats and model parameters provided by the vendors are usually different and sometimes not compatible with a sensor model based on a perspective transformation. Our new sensor model is designed to be applicable to a large variety of sensors. Vendor-specific definitions are mapped to the definitions of our sensor model during data import. A rigorous model is employed for compensating systematic errors in the orbit and attitude data. In this paper, we present the sensor model and describe the way the vendor-specific definitions are mapped to the definitions of the new sensor model for Quickbird, SPOT 5 and ALOS/PRISM. First results for the correction of systematic errors will be given for Quickbird and SPOT 5 for test sites in Melbourne and Bhutan.

## 1. INTRODUCTION

In order to exploit the full metric potential of high-resolution satellite imagery, it is necessary to develop appropriate sensor models. Nowadays most high-resolution optical satellite sensors are pushbroom scanners. For some of these sensors, camera replacement models with a set of rational polynomial coefficients (RPCs) are provided by the vendors. It has been shown that no loss in accuracy is to be expected when bias-corrected RPCs are used for georeferencing (Fraser & Hanley, 2003). However, not all vendors provide RPCs, and alternative models such as affine projection are not always applicable (e.g. for large image scenes or in mountainous terrain). In such cases, a sensor model that is more closely related to the physical reality of the imaging process has to be used.

A pushbroom scanner delivers a perspective image with individual exterior orientation parameters for each image line. These exterior orientation parameters are highly correlated and can be replaced by time-dependant models for the platform position and attitude angles. In the past a wide range of pushbroom sensor models with different intricacy have been developed. These sensor models differ both in the way that platform orbits and attitudes are modelled and in the models used for the correction of systematic errors. Some use simple curves for modelling the orbits, e.g. circles (Westin, 1990) or ellipses (Fritsch & Stallman, 2000), (Dowman & Michalis, 2003). Another strategy for modelling the imaging process is to assume the whole image to be one perspective image whose exterior orientation is modelled by the six parameters of a rigid motion. The difference between this simplified model and the actual imaging process is modelled by additional parameters. For instance, the method described by Konecny et al. (1987),

which uses eight such additional parameters, has been applied to images from IKONOS and QuickBird (Jacobsen & Passini, 2003) and SPOT 5/HRS (Jacobsen, 2004). More generic sensor models use piecewise polynomial functions to model the sensor trajectory and attitudes. For instance, Poli (2005) uses second order piecewise polynomial functions. Her model is very general, but it requires observations of the orbit positions and attitudes to make its parameters determinable. Such observations are often provided by the satellite vendors in metadata files. Despite the fact that the sensor geometry is the same for all pushbroom scanners, the formats and definitions of these metadata are not always compatible. For instance, Poli (2005) reports relatively poor accuracies achieved for SPOT 5 data because the SPOT 5 metadata do not explicitly contain information about the interior orientation of the camera.

This paper presents a new generic pushbroom sensor model. It is the result of a comprehensive analysis of the models used by various vendors and should be applicable to a variety of pushbroom scanners. The vendor-specific definitions are mapped to the general model when the metadata are imported. The orbit and attitudes are modelled by cubic splines. The parameters of the sensor model are initialised from the metadata provided by the vendors. These parameters can be used directly (*direct georeferencing*). As they are contaminated by systematic errors, development of a model for the correction of these errors was also needed. The parameters of this correction model can be estimated in a least squares adjustment if a small number of ground control points (GPCs) is available. In this paper, we will present the new sensor model, the model used for the correction of systematic errors, and the way the vendor-specific definitions are mapped to the definitions of our model for QuickBird, SPOT 5, and ALOS PRISM. We will also present first results of

---

\* Corresponding author.

systematic error correction for QuickBird and SPOT 5 for test sites in Melbourne and Bhutan.

## 2. A GENERIC PUSHBROOM SENSOR MODEL

### 2.1 Coordinate Systems

To model the transformation process between image and object space, different coordinate systems need to be defined. First of all, we define the *object coordinate system* as a three dimensional right-handed, earth-centred Cartesian coordinate system  $[\mathbf{X}_{ECS}]$ . Depending on the satellite vendor, the object coordinate system can be an International Terrestrial Reference System (ITRS), WGS84, or any other earth centered system.

Next we introduce an *orbital coordinate system*  $[\mathbf{X}_O]$ . This is a time-dependant system with the origin defined by the satellite position  $\mathbf{S}(t)$  at time  $t$ . We define the axes of this system so that the  $Z_O$ -axis is parallel to  $\mathbf{S}(t_c)$ , where  $t_c$  is the acquisition time at the scene centre. The  $Y_O$ -axis is orthogonal to both  $\mathbf{S}(t_c)$  and the velocity vector at time  $t_c$ ,  $\mathbf{V}(t_c)$ .  $X_O$  completes the right handed orbital system. Thus, for reasons to be explained below, for all times  $t$ , the orbital coordinate system is just shifted along with  $\mathbf{S}(t)$  and is therefore only tangential at the scene centre. The unit vectors  $\mathbf{X}_O, \mathbf{Y}_O, \mathbf{Z}_O$  of the axes of the orbital coordinate system can be computed according to Equation 1:

$$\mathbf{Z}_O = \frac{\mathbf{S}(t_c)}{\|\mathbf{S}(t_c)\|} \quad \mathbf{Y}_O = \frac{\mathbf{Z}_O \times \mathbf{V}(t_c)}{\|\mathbf{Z}_O \times \mathbf{V}(t_c)\|} \quad \mathbf{X}_O = \frac{\mathbf{Y}_O \times \mathbf{Z}_O}{\|\mathbf{Y}_O \times \mathbf{Z}_O\|} \quad (1)$$

The *platform coordinate system* is fixed to the satellite. The transformation between the platform and the orbit systems is a time-dependant rotation that can be parameterized by the three angles (*roll, pitch, yaw*). The relation between the three coordinate systems introduced so far can be seen in Figure 1.

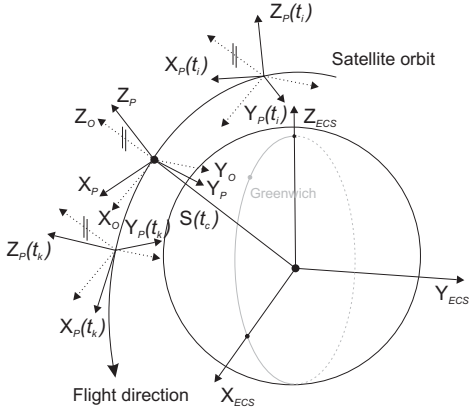


Figure 1. Coordinate systems  $[\mathbf{X}_{ECS}]$ ,  $[\mathbf{X}_O]$  and  $[\mathbf{X}_P]$ .

Inside the satellite body, the *camera coordinate system*  $[\mathbf{X}_C]$  has its origin in the projection centre  $C$ . The  $X_C$ -axis is parallel to the CCD array and the  $Y_C$ -axis is parallel to the focal plane. The  $Z_C$ -axis completes the right handed system. The relation between the camera and the platform system is given by the time-constant camera mounting parameters.

The *framelet coordinate system*  $[\mathbf{X}_F]$  is shifted relative to the camera system so that its origin is the centre of the leftmost pixel of the CCD array, but it is not rotated. The actual image observations  $(x_F, y_F)$  are taken in the framelet coordinate system.

As the satellite passes over the earth's surface, the CCD array records one image line after the other. These lines are concatenated to an image data file. The *image file coordinate system*  $[\mathbf{X}_I]$  is a system defined by the rows and columns of the image data file. Thus,  $x_I$  is identical to  $x_F$  (and corresponds to the column index of the digital image). The coordinate  $y_I$  (the row index) is used to compute the time  $t$  at which that image line was recorded, so that  $y_F$  is actually 0 at time  $t$ . Figure 2 shows the relationship between the second group of coordinate systems and the platform system.

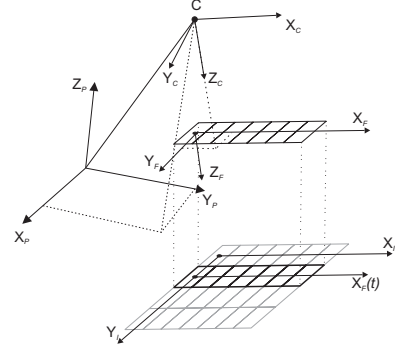


Figure 2. Coordinate systems  $[\mathbf{X}_P]$ ,  $[\mathbf{X}_C]$ ,  $[\mathbf{X}_F]$  and  $[\mathbf{X}_I]$ .

### 2.2 Transformations

The sensor model has to describe the transformation relating the position of a point  $\mathbf{P}_{ECS} = (X_{ECS}, Y_{ECS}, Z_{ECS})^T$  in the object coordinate system to the position of its projection  $\mathbf{p}_I = (x_I, y_I, 0)^T$  in the image file coordinate system. Measuring an image point  $\mathbf{p}_I$  immediately delivers the corresponding point  $\mathbf{p}_F$  in the framelet coordinate system:

$$\mathbf{p}_F = (x_F, y_F, z_F)^T = (x_I, 0, 0)^T \quad (2)$$

The coordinate  $y_I$  is used to compute the time  $t$  at which the image line containing the point was recorded:

$$t = t_0 + \Delta t \cdot y_I \quad (3)$$

In Equation 3,  $t_0$  is the acquisition time of the first image line, and  $\Delta t$  is the acquisition time per image line. These parameters are usually provided by the vendor in metadata files. Each image line is a central projection of the earth surface recorded at time  $t$ . Let the position of the projection centre in the framelet coordinate system be  $\mathbf{c}_F = (x_F^C, y_F^C, f)^T$ . Its components are usually referred to as the parameters of inner orientation:  $(x_F^C, y_F^C)$  are the coordinates of the principal point and  $f$  is the focal length. The camera coordinates of the image point are  $\mathbf{p}_C = \mathbf{p}_F - \mathbf{c}_F$ . The object point has to be situated on a straight line through the projection centre, and  $\mathbf{p}_C$  gives the direction from the projection centre to the object point in the camera coordinate system. Thus, the relationship between the object point  $\mathbf{P}_C$  in the camera coordinate system and the image point  $\mathbf{p}_F$  in the framelet coordinate system can be described as follows:

$$\mathbf{P}_C = (X_C, Y_C, Z_C)^T = \lambda \cdot (\mathbf{p}_F - \mathbf{c}_F + \delta \mathbf{x}) \quad (4)$$

In Equation 4,  $\lambda$  is a scale factor describing the position of  $\mathbf{P}_C$  along the image ray, and  $\delta \mathbf{x}$  is a vector describing corrections for systematic errors. In the current version,  $\delta \mathbf{x}$  comprises correction terms for velocity aberration (Digital Globe, 2006) and atmospheric refraction (Noerdlinger, 1999), but in the future it will be expanded to also model the camera distortion.

In order to transform  $\mathbf{P}_C$  to the platform system we apply the camera mounting parameters in the form of a rigid motion:

$$\mathbf{P}_P = (X_P, Y_P, Z_P)^T = \mathbf{C}_M + \mathbf{R}_M \cdot \mathbf{P}_C \quad (5)$$

In Equation 5, the camera mounting parameters are the position  $\mathbf{C}_M$  of the projection centre in the platform system, and the rotation matrix  $\mathbf{R}_M$  describing the rotation from the camera system to the platform system. The platform and orbital systems are related by a time-dependant rotation:

$$\mathbf{P}_O = (X_O, Y_O, Z_O)^T = \mathbf{R}_P(t) \cdot \mathbf{P}_P \quad (6)$$

The rotation matrix  $\mathbf{R}_P(t)$  is parameterised by three rotation angles (*roll*, *pitch*, *yaw*) changing with time, thus  $\mathbf{R}_P(t) = \mathbf{R}_P[\text{roll}(t), \text{pitch}(t), \text{yaw}(t)]$ . The continuous model for these three time-dependant angles will be described in Section 2.3. The time  $t$  used to evaluate the functions [*roll*( $t$ ), *pitch*( $t$ ), *yaw*( $t$ )] is derived from Equation 3.

Finally, the relationship between the object coordinates  $\mathbf{P}_{ECS}$  and the orbit coordinates  $\mathbf{P}_O$  is described by a rigid motion with a time-constant rotation matrix  $\mathbf{R}_O$  and a time-dependant shift given by the satellite position  $\mathbf{S}(t)$ :

$$\mathbf{P}_{ECS} = (X_{ECS}, Y_{ECS}, Z_{ECS})^T = \mathbf{S}(t) + \mathbf{R}_O \cdot \mathbf{P}_O \quad (7)$$

The columns of the rotation matrix  $\mathbf{R}_O$  are identical to the unit vectors of the orbital coordinate system as described by Equation 1. Hence there is a dependence on the acquisition time  $t_C$  of the image centre:  $\mathbf{R}_O = \mathbf{R}_O(t_C) = [\mathbf{X}_O(t_C) \ \mathbf{Y}_O(t_C) \ \mathbf{Z}_O(t_C)]$ . The continuous model for  $\mathbf{S}(t)$  will be described in section 2.3.

A combination of Equations 4 to 7 yields the transformation equation relating the image point  $\mathbf{p}_F$  in the framelet coordinate to the object point  $\mathbf{P}_{ECS}$  in the object coordinate system:

$$\mathbf{P}_{ECS} = \mathbf{S}(t) + \mathbf{R}_O \cdot \mathbf{R}_P(t) \cdot [\mathbf{C}_M + \lambda \cdot \mathbf{R}_M \cdot (\mathbf{p}_F - \mathbf{c}_F + \delta \mathbf{x})] \quad (8)$$

Using  $\mu = 1/\lambda$ , the inverse transformation can be expressed as:

$$\mathbf{p}_F = \mathbf{c}_F + \mu \cdot \mathbf{R}_M^T \cdot \{\mathbf{R}_P^T(t) \cdot \mathbf{R}_O^T \cdot [\mathbf{P}_{ECS} - \mathbf{S}(t)] - \mathbf{C}_M\} - \delta \mathbf{x} \quad (9)$$

### 2.3 Modelling the Satellite Orbit and Attitudes

The components  $X(t), Y(t), Z(t)$  of the satellite orbit  $\mathbf{S}(t)$  and the rotation angles *roll*( $t$ ), *pitch*( $t$ ), *yaw*( $t$ ) by which the rotation matrix  $\mathbf{R}_P$  is parameterised are modelled by cubic splines, i.e., by cubic polynomial segments  $Sp_N^i(\bar{t}_i)$  with smooth transitions between segments  $i$  and  $i+1$ :

$$Sp_N^i(\bar{t}_i) = a_{N,0}^i + a_{N,1}^i \cdot \bar{t}_i + a_{N,2}^i \cdot \bar{t}_i^2 + a_{N,3}^i \cdot \bar{t}_i^3 \quad (10)$$

In Equation 10,  $i$  is the index of the spline segment,  $N$  is the parameter modelled by the spline ( $X, Y, Z, \text{roll}, \text{pitch}$ , or *yaw*), and  $(a_{N,0}^i, a_{N,1}^i, a_{N,2}^i, a_{N,3}^i)$  are polynomial coefficients that have to be determined from observed orbit points or attitudes, respectively. Each polynomial  $Sp_N^i(\bar{t}_i)$  models the parameter  $N$  for a time interval  $[t_i^0, t_i^E]$  with  $t_i^E = t_{i+1}^0$  being the time of transition between segments  $i$  and  $i+1$ . The intervals  $[t_i^0, t_i^E]$  are mapped to  $[\bar{t}_i^0, \bar{t}_i^E] = [0, 1]$  using  $\bar{t}_i = (t - t_i^0)/(t_i^E - t_i^0)$ . At the interval limits, the two polynomials and their first and second derivatives have to be identical, which results in three constraint equations per inner node  $\bar{t}_{i+1}^0 = 0$  with  $i \neq 0$ :

$$\begin{aligned} 0 &= a_{N,0}^i + a_{N,1}^i + a_{N,2}^i + a_{N,3}^i - a_{N,0}^{i+1} \\ 0 &= a_{N,1}^i + 2 \cdot a_{N,2}^i + 3 \cdot a_{N,3}^i - a_{N,1}^{i+1} \\ 0 &= 2 \cdot a_{N,2}^i + 6 \cdot a_{N,3}^i - 2 \cdot a_{N,2}^{i+1} \end{aligned} \quad (11)$$

The satellite image vendors usually provide discrete orbit points and attitude observations with a time stamp. Some (but not all) vendors also provide information about the accuracy of these data. Let such an orbit point be  $(X^{obs}, Y^{obs}, Z^{obs})^T$ , recorded at time  $t^{obs}$ . Then by using  $t^{obs}$ , the segment  $i$  of the orbit splines that this point belongs to can be determined, and the relationship between the observed orbit coordinates and the orbit splines becomes

$$\begin{aligned} F_X(X^{obs}, Y^{obs}, Z^{obs}, t^{obs}) &= X^{obs} + \Delta X = Sp_X^i(\bar{t}_i^{obs}) \\ F_Y(X^{obs}, Y^{obs}, Z^{obs}, t^{obs}) &= Y^{obs} + \Delta Y = Sp_Y^i(\bar{t}_i^{obs}) \\ F_Z(X^{obs}, Y^{obs}, Z^{obs}, t^{obs}) &= Z^{obs} + \Delta Z = Sp_Z^i(\bar{t}_i^{obs}) \end{aligned} \quad (12)$$

In Equation 12,  $F_X$ ,  $F_Y$ , and  $F_Z$  are functions modelling systematic errors in the observed orbit coordinates. We currently model perturbations to the observed orbit coordinates as a time-constant shift only. Thus, the vector  $(\Delta X, \Delta Y, \Delta Z)^T$  describes a systematic shift of the system in which the observed orbit points are given relative to the object coordinate system. The more general notation of  $F_X, F_Y$ , and  $F_Z$  should indicate that in the future this model might be expanded, for instance by rotations or time-dependant terms. An analogous model is used for the attitudes. Perturbations in the observed rotation angles (*roll*<sup>obs</sup>, *pitch*<sup>obs</sup>, *yaw*<sup>obs</sup>)<sup>T</sup> are modelled by time-constant offsets  $(\Delta \text{roll}, \Delta \text{pitch}, \Delta \text{yaw})^T$ , a model that might be expanded by time-dependant terms in the future.

When the observed orbit points and attitudes are imported, the splines are initialised, and approximate values for the spline coefficients are determined. This is done by least squares adjustment, using Equation 12 as the original observation equations, but assuming that no systematic errors are present. The constraint Equations 11 are also considered. First, only one adjusting spline segment is used. If the rms error of the weight unit  $s_0$  of that adjustment exceeds a threshold, each spline segment is split into two segments of equal length. This procedure is iteratively applied until  $s_0$  is smaller than the threshold. Depending on the scene size, this will result in one or two segments for both the orbits and the attitudes.

### 2.4 Adjustment and Correction of Systematic Errors

It is the goal of the overall adjustment to determine the mapping parameters in the functional model described by Equation 9 and, as far as the models for the orbits and attitudes are concerned, Equation 10 from the framelet and object coordinates of GCPs and from the observed orbit and attitude coordinates provided by the vendor. Least squares adjustment is based on the Gauss-Helmert model. This model assumes that the observations  $\mathbf{l}$ , the corrections to these observations  $\mathbf{v}$ , and the unknown parameters  $\mathbf{x}$  are linked by constraint equations  $\mathbf{f}(\mathbf{l} + \mathbf{v}, \mathbf{x}) = \mathbf{0}$ , where  $\mathbf{f}$  are functions describing the functional model of adjustment. Additionally, there may be constraint equations only affecting the unknowns, in the form  $\mathbf{h}(\mathbf{x}) = \mathbf{0}$ . The unknown parameters  $\mathbf{x}$  are solved from the constraint equations by least squares adjustment.

For the observed image points, the functional model is given by the combination of Equations 9 and 10. In Equation 9, the

observations are the framelet coordinates  $\mathbf{p}_F$ . The camera mounting parameters will normally not be determinable at all, and they are kept constant. The corrections  $\delta\mathbf{x}$  are applied to the image coordinates, but they are also constant in the adjustment. The interior orientation parameters might be determinable for scenes covering undulating terrain, but in the current version of the model they are considered constant, as is the rotation matrix  $\mathbf{R}_O$ . Only the polynomial coefficients  $a_{N,0}^i$ ,  $a_{N,1}^i$ ,  $a_{N,2}^i$ , and  $a_{N,3}^i$  of the splines modelling the three components of the orbit  $\mathbf{S}(t)$  and the three angles by which  $\mathbf{R}_p(t)$  is parameterised have to be determined by adjustment. The positions  $\mathbf{P}_{ECS}$  of the GCPs are also considered to be unknown. That means that the GCP coordinates are used as direct observations for the unknown object coordinates, and they will receive residuals. The coefficients of polynomial coefficients of two neighbouring spline segments  $i$  and  $i + 1$  are linked by Equations 11, which are introduced as constraint equations. For the direct observations for the orbit points, the combination of Equations 10 and 12 provide the functional model. The observations in these equations are the orbit point coordinates ( $X^{obs}$ ,  $Y^{obs}$ ,  $Z^{obs}$ ) or the observed rotation angles ( $roll^{obs}$ ,  $pitch^{obs}$ ,  $yaw^{obs}$ ). The polynomial coefficients of the orbit and attitude splines are to be determined. With respect to the bias correction parameters ( $\Delta X$ ,  $\Delta Y$ ,  $\Delta Z$  and  $\Delta roll$ ,  $\Delta pitch$ ,  $\Delta yaw$ ), the user can decide whether to consider them constant (and zero) or unknown.

### 3. APPLICATIONS TO DIFFERENT SATELLITES

#### 3.1 QuickBird

For QuickBird, the transformation parameters provided in the metadata file relate the object coordinates  $\mathbf{P}_{ECS}$  of a point to its *detector coordinates*  $\mathbf{p}_D$  (Digital Globe, 2006). This coordinate system is defined in a similar way as the framelet coordinate system used in our model, but it is rotated by 90 degrees around the  $Z_F$ -axis, thus  $x_F = -y_D$  and  $y_F = x_D$  or:

$$\mathbf{p}_D = \mathbf{R}_{Z90}^T \cdot \mathbf{p}_F \quad (13)$$

The relation between  $\mathbf{P}_{ECS}$  and  $\mathbf{p}_F$  according to Digital Globe (2006) can formally be written as:

$$\mathbf{P}_{ECS} = \mathbf{S}(t) + \mathbf{R}_Q^T(t) \cdot [\mathbf{C}_{MQ} + \lambda \cdot \mathbf{R}_{MQ}^T \cdot (\mathbf{R}_C^T \cdot \mathbf{R}_{Z90}^T \cdot \mathbf{p}_F + \mathbf{p}_F^0 + \delta\mathbf{x}_Q)] \quad (14)$$

In Equation 14, the index  $Q$  denotes a QuickBird-specific definition of a parameter. Comparing Equations 8 and 14, we can observe several differences. First, there is no orbit coordinate system and thus no rotation matrix  $\mathbf{R}_O$ . The rotation matrices as defined in Digital Globe (2006) are transposed compared to those appearing in Equation 8, and  $\mathbf{R}_Q(t)$  and  $\mathbf{R}_{MQ}$  are parameterised by quaternions. The framelet coordinate system is not only rotated by  $\mathbf{R}_{Z90}^T$ , but also by a rotation  $\mathbf{R}_C^T$  around the  $Z_F$ -axis. Instead of the framelet coordinates  $\mathbf{c}_F$  of the projection centre, the coordinates  $\mathbf{p}_C^0$  of the origin of the framelet coordinate system in the QuickBird camera system are given. Finally, the corrections  $\delta\mathbf{x}_Q$  are applied in the camera coordinate system. Equation 14 can be re-written as:

$$\mathbf{P}_{ECS} = \mathbf{S}(t) + \mathbf{R}_Q^T(t) \cdot [\mathbf{C}_{MQ} + \lambda \cdot \mathbf{R}_{MQ}^T \cdot \mathbf{R}_C^T \cdot \mathbf{R}_{Z90}^T \cdot (\mathbf{p}_F + \mathbf{R}_{Z90} \cdot \mathbf{R}_C \cdot \mathbf{p}_F^0 + \mathbf{R}_{Z90} \cdot \mathbf{R}_C \cdot \delta\mathbf{x}_Q)] \quad (15)$$

A comparison of Equations 8 and 15 results in formulae for determining  $\mathbf{c}_F$  and  $\delta\mathbf{x}$  from the parameters given in the QuickBird metadata files:

$$\mathbf{c}_F = -\mathbf{R}_{Z90} \cdot \mathbf{R}_C \cdot \mathbf{p}_F^0 \quad (16)$$

$$\delta\mathbf{x} = \mathbf{R}_{Z90} \cdot \mathbf{R}_C \cdot \delta\mathbf{x}_Q \quad (17)$$

The rotation matrix  $\mathbf{R}_Q^T(t)$  in Equation 14 rotates from the object coordinate system to a system whose  $Z$ -axis points to the target, i.e., that system is not a tangential one. The rotation matrix  $\mathbf{R}_{MQ}^T \cdot \mathbf{R}_C^T \cdot \mathbf{R}_{Z90}^T$  rotates into the camera coordinate system. We have to split  $\mathbf{R}_Q^T(t)$  into two rotations, and we want the platform coordinate system to be close to a tangential system, which means that we cannot use the otherwise obvious identity  $\mathbf{R}_M = \mathbf{R}_{MQ}^T \cdot \mathbf{R}_C^T \cdot \mathbf{R}_{Z90}^T$ . Rather than that, we define the rotation matrix  $\mathbf{R}_p(t)$  to be equal to the identity matrix for the acquisition time  $t_c$  of the image centre, thus  $\mathbf{R}_p(t_c) = \mathbf{I}$ . The matrix  $\mathbf{R}_O$  in Equation 8 is computed from the orbit positions and velocities at time  $t_c$ . A comparison of Equations 8 and 15, which accounts for the overall rotation between the camera and the object coordinate systems being identical, yields for  $t = t_c$ :

$$\mathbf{R}_Q^T(t_c) \cdot \mathbf{R}_{MQ}^T \cdot \mathbf{R}_C^T \cdot \mathbf{R}_{Z90}^T = \mathbf{R}_O \cdot \mathbf{R}_p(t_c) \cdot \mathbf{R}_M = \mathbf{R}_O \cdot \mathbf{I} \cdot \mathbf{R}_M \quad (18)$$

Thus the camera mounting rotation matrix  $\mathbf{R}_M$  can be computed from the parameters given in the QuickBird metadata files:

$$\mathbf{R}_M = \mathbf{R}_O^T \cdot \mathbf{R}_Q^T(t_c) \cdot \mathbf{R}_{MQ}^T \cdot \mathbf{R}_C^T \cdot \mathbf{R}_{Z90}^T \quad (19)$$

Using the shorthand  $\mathbf{p}_C = \mathbf{p}_F + \mathbf{R}_{Z90} \cdot \mathbf{R}_C \cdot \mathbf{p}_F^0 + \mathbf{R}_{Z90} \cdot \mathbf{R}_C \cdot \delta\mathbf{x}_Q$ , Equation 15 can be re-written as

$$\begin{aligned} \mathbf{P}_{ECS} &= \mathbf{S}(t) + \mathbf{R}_Q^T(t) \cdot \mathbf{R}_Q(t_c) \cdot \mathbf{R}_O \cdot [\mathbf{R}_O^T \cdot \mathbf{R}_Q^T(t_c) \cdot \mathbf{C}_{MQ} + \\ &\quad + \lambda \cdot \mathbf{R}_O^T \cdot \mathbf{R}_Q^T(t_c) \cdot \mathbf{R}_{MQ}^T \cdot \mathbf{R}_C^T \cdot \mathbf{R}_{Z90}^T \cdot \mathbf{p}_C] \\ &= \mathbf{S}(t) + \mathbf{R}_Q^T(t) \cdot \mathbf{R}_Q(t_c) \cdot \mathbf{R}_O \cdot [\mathbf{R}_O^T \cdot \mathbf{R}_Q^T(t_c) \cdot \mathbf{C}_{MQ} + \lambda \cdot \mathbf{R}_M \cdot \mathbf{p}_C] \quad (20) \end{aligned}$$

A comparison between Equations 8 and 20 delivers the remaining parameters in Equation 8:

$$\mathbf{C}_M = \mathbf{R}_O^T \cdot \mathbf{R}_Q^T(t_c) \cdot \mathbf{C}_{MQ} \quad (21)$$

$$\mathbf{R}_p(t) = \mathbf{R}_O^T \cdot \mathbf{R}_Q^T(t) \cdot \mathbf{R}_Q(t_c) \cdot \mathbf{R}_O \quad (22)$$

Equation 22 has to be applied to each of the discrete data points provided for the satellite attitudes, and the angles  $roll^{obs}(t)$ ,  $pitch^{obs}(t)$ ,  $yaw^{obs}(t)$  derived from  $\mathbf{R}_p(t)$  are used in the adjustment.

#### 3.2 SPOT 5

For SPOT 5, the definition of the transformation parameters provided in the metadata file relates the object coordinates  $\mathbf{P}_{ECS}$  of a point to its *navigation coordinates*  $\mathbf{P}_{PS}$  (SPOT, 2002). The navigation coordinate system is related to our platform coordinate system by a rotation  $\mathbf{R}_T$ :

$$\mathbf{P}_P = \mathbf{R}_T \cdot \mathbf{P}_{PS}, \quad \mathbf{R}_T = \begin{pmatrix} 0 & -1 & 0 \\ 1 & 0 & 0 \\ 0 & 0 & 1 \end{pmatrix} \quad (23)$$

According to SPOT (2002), the relationship between  $\mathbf{P}_{ECS}$  and  $\mathbf{P}_P$  can formally be written as:

$$\mathbf{P}_{ECS} = \mathbf{S}(t) + \lambda \cdot \mathbf{R}_{OS}(t) \cdot \mathbf{R}_{PS}(t) \cdot \mathbf{R}_T^T \cdot \mathbf{P}_P \quad (24)$$

There are two main differences to our definitions. First of all, there are two time-dependent rotations. The rotation  $\mathbf{R}_{OS}(t)$  is computed in the same way as  $\mathbf{R}_O$  from the satellite orbit and velocity vectors, but individually for each time  $t$ . Using the definition for  $\mathbf{R}_O$  described in Section 2.2 and comparing Equations 8 and 24 results both in  $\mathbf{C}_M = \mathbf{0}$  and in the following equation for computing  $\mathbf{R}_p(t)$  from the parameters provided in the SPOT 5 metadata files:

$$\mathbf{R}_p(t) = \mathbf{R}_O^T \cdot \mathbf{R}_{OS}(t) \cdot \mathbf{R}_{PS}(t) \cdot \mathbf{R}_T^T \quad (25)$$

The second major difference is the description of interior orientation parameters which are available only in an indirect way through the definition of two viewing angles  $\psi_x$  and  $\psi_y$  that are related to  $\mathbf{P}_{PS}$  by  $\mathbf{P}_{PS} = [-\tan(\psi_y), \tan(\psi_x), 1]^T$  (SPOT, 2002) and, thus, to  $\mathbf{P}_p = [\tan(\psi_x), \tan(\psi_y), -1]^T$  as a geometrical positive. The angles  $\psi_x$  and  $\psi_y$  are provided for each pixel of the CCD array and define a bundle of rays between the projection centre and the pixel centres of the CCD array (Figure 3).

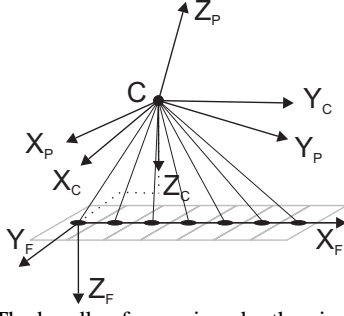


Figure 3. The bundle of rays given by the viewing angles.

Using the relationship between  $\mathbf{P}_p$  and the viewing angles defined above, and applying Equations 4 and 5 with  $\delta\mathbf{x} = \mathbf{0}$ , yields the relationship between the viewing angles  $\psi_x$  and  $\psi_y$  provided in the SPOT 5 metadata files and the interior orientation  $\mathbf{c}_F$  and mounting rotation  $\mathbf{R}_M$  used in our model (Equation 8):

$$\mathbf{P}_p = [\tan(\psi_x), \tan(\psi_y), -1]^T = \nu \cdot \mathbf{R}_M \cdot (\mathbf{p}_F - \mathbf{c}_F) \quad (26)$$

For each pixel of the CCD array,  $\mathbf{p}_F$  and  $\mathbf{P}_p$  are known. This means that the rotation angles by which  $\mathbf{R}_M$  is parameterised and  $\mathbf{c}_F$  can be computed by a spatial resection, using Equation 26 as the basis for the functional model of the adjustment. However, as all the points lie on a straight line in the platform system, one rotation angle will not be defined. Parameterising  $\mathbf{R}_M$  by (roll, pitch, yaw), the angle roll (around the  $X_F$ -axis) will not be determined. We set  $roll = 180^\circ = const$ . In order to eliminate the unknown scale parameter  $\nu$ , the first and the second component of Equation 26 can be divided by the third. Thus, for each pixel of the CCD array we obtain two observation equations to determine the angles pitch and yaw of  $\mathbf{R}_M$  and the interior orientation parameters  $\mathbf{c}_F$ . We get a highly redundant system of equations that is solved by least squares adjustment. This adjustment is carried out when the SPOT 5 metadata are imported.

### 3.3 ALOS PRISM

According to JAXA (2006), the transformation process between object and image space can be expressed by Equation 27:

$$\mathbf{P}_{ECS} = \mathbf{S}(t) + \mathbf{R}_A(t) \cdot [\mathbf{C}_M + \lambda \cdot \mathbf{R}_M \cdot (\mathbf{p}_F - \mathbf{c}_F + \delta\mathbf{x})] \quad (27)$$

This is very similar to Equation 8. The only difference is that there is only one rotation  $\mathbf{R}_A(t)$  relating the platform and object coordinate systems, and this rotation matrix is parameterised by quaternions. Computation of the rotation matrix  $\mathbf{R}_O$  described in Section 2.2, using the identity  $\mathbf{R}_O \cdot \mathbf{R}_p(t) = \mathbf{R}_A(t)$ , results in:

$$\mathbf{R}_p(t) = \mathbf{R}_O^T \cdot \mathbf{R}_A(t) \quad (28)$$

With ALOS PRISM, there is one speciality with respect to the framelet coordinate system. Depending on the viewing mode, either 4 or 6 CCD arrays are used to record the digital image. For basic imagery, one image data file per CCD array is provided. Figure 4 illustrates the configuration of 4 such CCD arrays. There is an individual framelet coordinate system for each CCD array. All parameters in the model in Equation 8 are identical for each of these framelet coordinates except the coordinates of the principal point ( $x_F^C, y_F^C$ ): they differ by a constant offset, defined by the widths of the CCD arrays and the nominal overlap of 32 pixels. The import of the metadata for ALOS has not been implemented because the documentation of the binary metadata format appears incomplete, and precise information is difficult to obtain. Once it has been implemented, tests will show whether the nominal overlap can be trusted or whether it will be necessary to determine individual coordinates of the principal point and/or individual distortion parameters for each of the image data files.

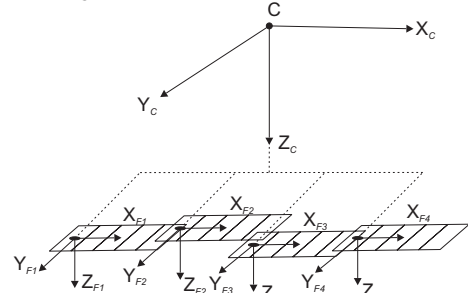


Figure 4. CCD array configuration of ALOS Prism

## 4. EXPERIMENTS

### 4.1 Test data

For the testing of our model for SPOT 5, we used a pan-chromatic image with 2.5 m resolution, covering an area of 60 x 60 km<sup>2</sup> in Bhutan. We determined 61 points using GPS, of which 7 were used as GCPs. The remaining 54 points were used as check points. The distribution of the points was not optimal due to the restricted accessibility of the terrain. Points were mainly located along roads on valley floors, with a few on passes, the overall height range being from 1200 m to 3800 m. The accuracy of the GPS coordinates was around  $\pm 0.2$  m in planimetry and  $\pm 0.4$  m in height. In order to test our model for QuickBird we used a pan-chromatic image of Melbourne covering an area of 18.7 x 18 km<sup>2</sup> at 0.8 m resolution. For this test field, 32 points were determined using GPS with an accuracy of  $\pm 0.1$  m in all coordinates. Of these points, 5 were used as control points and 27 as check points. Here we had a good point distribution in the scene centre, but no points at the periphery of the image. Many of the points are roundabouts, which were measured with an ellipse fitting technique both in object space as well as in image space. The terrain was flat with heights between 0 m and 80 m.

### 4.2 Results

Table 1 presents the results of the estimation of the interior orientation and the camera mounting rotations for the SPOT 5 image. The precision of the interior orientation is in the range of  $\pm 2$  pixel. The residuals of the adjustment are all below 0.05 pixels, so that no additional parameters seem to be necessary. An analysis of the covariance matrix of the parameters shows a high correlation between  $y_F^C$  and pitch.

	$x_F^C$ [pixel]	$y_F^C$ [pixel]	$f$ [pixel]	$Pitch$ [°]	$Yaw$ [°]
Value	11618.5	-2994.9	332912.2	15.0675	89.9945
$\sigma$	1.6	2.0	1.8	$3.1 \cdot 10^{-4}$	$1.8 \cdot 10^{-4}$

Table 1. Interior orientation and camera mount rotations for SPOT 5.  $\sigma$ : theoretical standard error.

In order to assess the effectiveness of our adjustment model, we measured the image coordinates of both the GCPs and the check points in both test images. First, we back-projected all check-points to the images using the original parameters of our sensor model, i.e., those derived by mapping the vendor-specific parameters to our model. We computed the RMS errors of the coordinate differences. These RMS errors show the accuracy achieved by direct georeferencing. We also carried out three different versions of adjustment, determining different groups of correction parameters. First, we determined only the orbit shift corrections. Second, only the attitude corrections, and third, both corrections were determined. The check points were back-projected to the images using the improved parameters, and the RMS errors of the coordinate differences were computed. The improvement in the RMS errors should show the effectiveness of the correction technique. For QuickBird, we also used the bias corrected RPC model for back-projection.

Correction	QuickBird [pixel]			SPOT 5 [pixel]		
	X	Y	X+Y	X	Y	X+Y
None	9.53	14.68	12.38	1.57	11.10	7.93
Shift	0.40	0.60	0.51	0.99	1.01	1.00
Attitudes	0.42	0.68	0.56	1.03	0.99	1.01
Orbit Shift + Attitudes	0.39	0.64	0.53	0.96	0.96	0.96
RPC	0.33	0.50	0.43	N/A	N/A	N/A

Table 2. RMS errors of the differences between back-projected and measured check-point coordinates for different variants of systematic error correction. RPC: bias corrected RPCs. Number of GCPs / check points: 5 / 27(QuickBird), 7 / 54 (SPOT 5).

Table 2 shows the results of these tests. The RMS error of coordinate for direct georeferencing is  $\pm 12.4$  pixels for QuickBird and  $\pm 7.9$  pixels for SPOT 5, thus clearly showing the importance of correcting the systematic errors in order to exploit the full metric potential of the imagery. Bias correction improves the results considerably. For the QuickBird scene, a RMS error of  $\pm 0.5$  pixels shows that subpixel accuracy can be achieved for well-defined points. The bias corrected RPC parameters achieve a slightly better result. This indicates that our correction model can still be improved, e.g. by adding a rotation to the correction of the orbit path, or by adding time-dependant terms to the attitude corrections. The results in Table 2 are almost independent of the type of bias correction. This is caused by the fact that these parameters cannot be separated well using such a small number of GCPs. For SPOT 5, the RMS error is reduced to  $\pm 1$  pixel by the bias correction. This is not quite as good as for QuickBird, but the check points in Bhutan were not as well defined as those in Melbourne, so that this larger RMS error is the result of the random measurement errors rather than of a remaining bias in the parameters of the sensor model.

## 5. CONCLUSIONS

A new generic pushbroom sensor model for high-resolution satellite images has been developed. The model should be applicable to most pushbroom scanners. In order to apply the model to images from a specific sensor, the vendor-specific parameterisation of the transformations has to be mapped to that used by our model. The way in which this can be achieved has been shown for QuickBird, SPOT 5 and ALOS PRISM. In the case of SPOT 5, this requires an initial adjustment to determine the interior orientation and the camera mount rotations. Also, a bias correction model has been implemented and tested. It was shown that by correcting the orbit shifts and attitudes using our model, an accuracy of  $\pm 1$  pixel or better can be achieved for QuickBird and SPOT 5 imagery.

## REFERENCES

- JAXA, 2006. ALOS Product Format Description. [http://stage.tksc.jaxa.jp/eorcalos/PRISM\\_L1\\_J\\_ENa.zip](http://stage.tksc.jaxa.jp/eorcalos/PRISM_L1_J_ENa.zip), (accessed 07 Apr. 2007)
- Digital Globe, 2006. QuickBird Imagery Products – Product Guide. <http://www.digitalglobe.com/downloads/QuickBirdImageryProducts-ProductGuide.pdf>, (accessed 07 Apr. 2007)
- Dowman, I., Michalis P., 2003. Generic rigorous model for along track stereo satellite sensors. Proceedings of ISPRS Workshop “High Resolution Mapping from Space 2003”, Hannover, Germany. Proceedings on CDROM
- Fraser, C., Hanley H., 2003. Bias compensation in rational functions for IKONOS satellite imagery. PE&RS 69(1): 53-57.
- Fritsch, D., Stallman D., 2000. Rigorous photogrammetric modelling processing of high resolution satellite imagery. IAPRS, 33-B1, Amsterdam, pp. 313-312.
- Jacobsen, K., Passini, R., 2003. Accuracy of digital orthophotos from high resolution space imagery. Proceedings of ISPRS Workshop “High Resolution Mapping from Space 2003”, Hannover, Germany. Proceedings on CDROM
- Jacobsen, K., 2004. DEM Generation by SPOT HRSC. IAPRS 35-B1, Istanbul, Turkey, pp. 439-444.
- Noerdlinger, P., 1999 Atmospheric refraction effects in Earth remote sensing. ISPRS Journal of Photogrammetry & Remote Sensing 54 (1999), pp. 360-373.
- Konecny, G., Lohmann P, Engel H., Kruck E. 1987. Evaluation of SPOT imagery on analytical Photogrammetric instrument. PE&RS 53(9), pp.1223-1230.
- Poli, D., 2005 Modelling of Spaceborne Liner Array Sensors. Ph. D. Dissertation, IGP Report No. 85, Institute of Geodesy and Photogrammetry, ETH Zurich, Switzerland.
- SPOT, 2002. SPOT Satellite Geometry Handbook. Reference S-NT-73-12-SI, Edition 1, Revision 0, Date 2002-01-15.
- Westin, T. 1990. Precision rectification of SPOT imagery. PE&RS 56(2), pp. 247-253.